



Extreme ozone depletion in the 2010–2011 Arctic winter stratosphere as observed by MIPAS/ENVISAT using a 2-D tomographic approach

E. Arnone¹, E. Castelli¹, E. Papandrea², M. Carlotti², and B. M. Dinelli¹

¹Istituto di Scienza dell'Atmosfera e del Clima – CNR, Bologna, Italy

²Dipartimento di Chimica Fisica e Inorganica, Università di Bologna, Bologna, Italy

Correspondence to: E. Arnone (e.arnone@isac.cnr.it)

Received: 26 July 2011 – Published in Atmos. Chem. Phys. Discuss.: 16 December 2011

Revised: 31 August 2012 – Accepted: 17 September 2012 – Published: 10 October 2012

Abstract. We present observations of the 2010–2011 Arctic winter stratosphere from the Michelson Interferometer for Passive Atmospheric Sounding (MIPAS) onboard ENVISAT. Limb sounding infrared measurements were taken by MIPAS during the Northern polar winter and into the subsequent spring, giving a continuous vertically resolved view of the Arctic dynamics, chemistry and polar stratospheric clouds (PSCs). We adopted a 2-D tomographic retrieval approach to account for the strong horizontal inhomogeneity of the atmosphere present under vortex conditions, self-consistently comparing 2011 to the 2-D analysis of 2003–2010. Unlike most Arctic winters, 2011 was characterized by a strong stratospheric vortex lasting until early April. Lower stratospheric temperatures persistently remained below the threshold for PSC formation, extending the PSC season up to mid-March, resulting in significant chlorine activation leading to ozone destruction. On 3 January 2011, PSCs were detected up to 30.5 ± 0.9 km altitude, representing the highest PSCs ever reported in the Arctic. Through inspection of MIPAS spectra, 83 % of PSCs were identified as supercooled ternary solution (STS) or STS mixed with nitric acid trihydrate (NAT), 17 % formed mostly by NAT particles, and only two cases by ice. In the lower stratosphere at potential temperature 450 K, vortex average ozone showed a daily depletion rate reaching $100 \text{ ppbv day}^{-1}$. In early April at 18 km altitude, 10 % of vortex measurements displayed total depletion of ozone, and vortex average values dropped to 0.6 ppmv. This corresponds to a chemical loss from early winter greater than 80 %. Ozone loss was accompanied by activation of ClO, associated depletion of its reservoir ClONO₂, and sig-

nificant denitrification, which further delayed the recovery of ozone in spring. Once the PSC season halted, ClO was reconverted primarily into ClONO₂. Compared to MIPAS observed 2003–2010 Arctic average values, the 2010–2011 vortex in late winter had 15 K lower temperatures, 40 % lower HNO₃ and 50 % lower ozone, reaching the largest ozone depletion ever observed in the Arctic. The overall picture of this Arctic winter was remarkably closer to conditions typically found in the Antarctic vortex than ever observed before.

1 Introduction

In the early 1980s, the discovery of a major ozone loss in the Antarctic spring (Farman et al., 1985), the so called ozone hole, led to an unprecedented international effort to understand and regulate the impact of ozone depleting substances on the protective ozone layer (WMO, 2011). The key mechanisms of ozone depletion were soon related to chlorine compounds and polar stratospheric clouds (PSCs) in the very cold and undisturbed Southern polar vortex (Solomon et al., 1986). The formation of nitric acid trihydrate (NAT), supercooled ternary solution (STS), and ice PSCs provides both the surfaces needed for heterogeneous chemistry and a means for removal of HNO₃ and H₂O through temporary capture and sedimentation (Solomon, 1999). Heterogeneous chemistry on PSC particles converts chlorine reservoirs ClONO₂ and HCl into Cl₂. In the sunlit Antarctic spring, chlorine molecules are converted into active radicals such as Cl and ClO, which destroy most of the vortex ozone at 14–20 km

altitude (Solomon et al., 1986; Molina et al., 1987; WMO, 2011). The destruction occurs at a much faster rate than the slow gas-phase nitrogen cycles driving depletion in the layers above. Additional reactions with BrO compounds contribute to ozone depletion in the lower stratosphere. Denitrification of the Antarctic stratosphere through sedimentation of HNO₃ prevents the reactive NO_x to promptly recapture the available chlorine into the ClONO₂ reservoir, which in turn would halt the depletion (see the review by Solomon, 1999). Radiative feedback of the Antarctic ozone hole was also proposed to further extend the persistence of low temperatures, significantly delaying the spring ozone recovery (Randel and Wu, 1999).

The same basic ozone depleting mechanisms are at play also in the Arctic (Solomon, 1999; WMO, 2011). The total ozone depletion in the Arctic winter was found to be linearly dependent on the volume of air having temperature below the threshold for PSC formation (V_{PSC}) integrated over the winter (Rex et al., 2006). The relationship was recently proved to apply also to individual stratospheric layers (Harris et al., 2010). Whereas in the Antarctic the V_{PSC} needed for complete ozone destruction in the lower stratosphere is exceeded every year (Tilmes et al., 2006), large planetary wave disturbances (Andrews et al., 1987) usually prevent very cold temperatures to persist in the Northern polar vortex, so that PSC occurrence in the Arctic is limited to smaller air volumes and shorter periods. As a consequence, ozone depletion in past Arctic winters did not reach the magnitude observed over the Antarctic. The observed Arctic total ozone loss in past years ranged between 25 and 35 % in very cold winters (such as in 1995–1996, 1999–2000 and 2004–2005) to almost none in warmer winters (WMO, 2011; Kuttippurath et al., 2010). In particular, 1995–1996 showed the coldest Arctic temperatures of the previous 17 yr extending until early March, with a column loss of 105 Dobson Units DU (Rex et al., 2006), or about 2/3 of that observed in Antarctic over an equivalent period (Manney et al., 1996). In 1999–2000 Arctic winter, ozone column loss was 88 DU but reached 70 % in a narrow layer of the lower stratosphere (Rex et al., 2002). In 2004–2005, ozone was affected by the largest loss (121 DU) reported for past winters (Rex et al., 2006), halted by a stratospheric warming in early March so that the magnitude of Antarctic ozone loss was not matched (e.g. Manney et al., 2006). Recently, close to Antarctic ozone hole conditions were reported for the 2010–2011 Arctic winter (Manney et al., 2011; Sinnhuber et al., 2011).

In this paper, we present observations of the 2010–2011 Arctic winter taken by the Michelson Interferometer for Passive Atmospheric Sounding (MIPAS) onboard the polar orbiting ENVISAT satellite (Fischer et al., 2008). MIPAS has proven to be a suitable instrument for detailed studies of polar stratospheric processes (see e.g. Glatthor et al., 2004; Stiller et al., 2005) including observation of PSCs and their composition (Spang et al., 2005; Höpfner et al., 2006). MIPAS observations were analysed with a 2-D tomographic re-

trieval (the Geofit Multi-Target Retrieval, GMTR, by Carlotti et al., 2006) to correctly account for along-track horizontal inhomogeneities. The resulting data (MIPAS2D, Dinelli et al., 2010) were proven to greatly reduce the spurious anomalies induced by horizontal gradients not accounted for by conventional 1-D codes (Kiefer et al., 2010), and are therefore more suitable under vortex conditions. The structure of the paper is as follows: Sect. 2 presents the MIPAS experiment, the MIPAS2D data, the PSC detection method, and the adopted meteorological products. MIPAS observations of the vortex dynamics, PSCs and chemical evolution of the Arctic stratosphere are presented in Sect. 3. The results are discussed in Sect. 4 in comparison to previous Arctic winters and typical Antarctic conditions. Conclusions are given in Sect. 5.

2 Data and methodology

2.1 MIPAS

MIPAS is part of the payload of Europe's Environmental monitoring satellite, ENVISAT, launched on 1 March 2002. ENVISAT was inserted into a polar orbit at an inclination of 81.5° and altitude of about 800 km. The orbital period is about 101 min achieving a global coverage of the Earth with 14.3 daily sun-synchronous orbits with the descending (North to South) part crossing the Equator at approximately 10:00 local time (LT) and the ascending part crossing it at approximately 22:00 LT (hereafter labelled am and pm measurements). MIPAS is a limb-scanning Fourier Transform (FT) spectrometer recording the emission of the atmosphere in the mid-infrared, with a spectral range extending from 680 to 2410 cm⁻¹ (14.6–4.15 μm) and an instantaneous field of view of approximately 3 km in height and 30 km across track at tangent point. Most of its measurements are taken with an along track backward looking configuration, with a sideward deviation at high latitudes allowing MIPAS to measure from pole to pole. During the original full resolution (FR) mission, MIPAS was operated with a spectral resolution of 0.035 cm⁻¹ full width half maximum (unapodised). The FR mission covers the time period from July 2002 to March 2004, when MIPAS operations in the original configuration were suspended due to the deterioration of the interferometric slides. Starting from January 2005, MIPAS operations have been resumed in the optimised resolution (OR) mission, with the instrument operating at 41 % of its maximum spectral resolution. The complete nominal limb scanning sequence (scan) of the original FR mission consists of 17 spectra with nominal tangent points ranging from 6 to 68 km, and a horizontal separation between adjacent scans of about 500 km (~4.6 degrees in latitude). In the OR nominal observation mode, each scan is made of 27 limb views with tangent altitudes ranging from 3 to 70 km at variable altitude steps. We also made use of the OR middle atmosphere observation

mode, spanning from 18 to 102 km altitude with 29 limb views at a constant 3 km step. The OR scan pattern corresponds to a horizontal separation between adjacent scans of about 410 km (~ 3.7 degrees in latitude). A more detailed description of the MIPAS experiment can be found in Fischer et al. (2008).

2.2 MIPAS2D data

We retrieved MIPAS level 2 products with the Geofit Multi-Target Retrieval (GMTR) tomographic analysis tool (Carlotti et al., 2006). GMTR is based on the Geo-fit approach (Carlotti et al., 2001) upgraded with the Multi-Target Retrieval (MTR) functionality (Dinelli et al., 2004). The Geo-fit approach enables to take into account horizontal atmospheric inhomogeneities by performing a tomographic retrieval on observations collected along a whole orbit through a 2-D discretization of the atmosphere. Since MIPAS lines of sight deviate from a backward alignment when approaching the poles, the 2-D approach assumes that the atmosphere is homogeneous across the orbit track. The maximum latitudinal component of this assumption for the lines of sight contributing to a portion of atmosphere is 2° latitude (Dinelli et al., 2010). The capability of the GMTR system to model the horizontal structures of the atmosphere makes its application to MIPAS measurements particularly suitable for the work presented in this paper that is focused on the polar winter regions, where strong horizontal gradients are present. The MTR approach, by simultaneously fitting pressure (p), temperature (T) and some interfering species, allows a reduction of the systematic error components due to the propagation of the uncertainties on p , T and on the amount of molecules that generate interfering spectral features. An upgraded version of the GMTR system was applied by Dinelli et al. (2010) to MIPAS observations to generate the MIPAS2D database. MIPAS2D can be found at <http://www.mbf.fci.unibo.it/mipas2d.html> and at <http://www.isac.cnr.it/~rss/mipas2d.htm> (hereafter MIPAS2D website). The MIPAS2D database consists of 2-D fields of p , T , and volume mixing ratio (VMR) of the six high priority species H_2O , O_3 , HNO_3 , CH_4 , N_2O , and NO_2 , covering the complete MIPAS mission. The database, thoroughly described in Dinelli et al. (2010) and Papandrea et al. (2010), has been used as a starting point for this analysis. The 2-D fields were obtained on a fixed vertical grid (spanning the altitude range from 6 to 42 km in steps of 3 km, and upward at altitudes of 47, 52, 60 and 68 km), and on a horizontal equispaced grid of 5° in latitude. Because of their correlations, p , T and H_2O were jointly retrieved with O_3 , followed by the sequential retrieval of the VMRs of the other molecules listed above.

For this work, we have upgraded the MIPAS2D database by analysing the newly delivered MIPAS level 1b data where both FR and OR missions were processed with the same Instrument Processing Facility version 5.05. This version was shown to improve the previous processing, and, most impor-

tantly, to lead to a correct altitude determination validated by comparison to radiosonde data (see e.g. Tomasi et al., 2011). Biases may be caused by the different retrieval configuration needed for the different spectral resolution of the FR and OR MIPAS measurements. To avoid this, the FR spectral resolution was numerically degraded to the resolution of the OR mission, so that the same set of spectral intervals (microwindows) could be used throughout the whole MIPAS mission. We also included observations from the middle atmosphere observation mode consistently retrieved with the same configuration as the nominal mode. Other modes were not included since they did not cover the lower stratosphere in 2010–2011, producing short data gaps. One-day data gaps were present in 2010 on 5, 15 and 25 December; and in 2011 on 4, 14, 24 January, 13, 23 February, 5, 15, 25 March; because the vortex had a very similar shape on adjacent days, time series were interpolated through these small data gaps. Data gaps of more than one day were clearly shown in the analysis.

The quality of MIPAS2D data for key species was described in Dinelli et al. (2010). Total systematic errors at the altitudes of interest for this study are: 3–8 % for p , 0.7–1.5 K for T , 5–7 % for ozone, and 5–20 % for the other species. Random errors are: 0.5–1.5 % for p , 0.2–0.3 K for T , 2–5 % for ozone, 2–10 % for the other species except for ClO whose random error values are of the order of 50 %. Reference average error profiles for the new processing of these key species are reported on the MIPAS2D website. The large error on ClO is due to its very weak spectral signal (often below the noise level). Averages of ClO data have been performed including only am measurements, with daylight conditions depending on the location of the measurement as compared to the day-night terminator. The influence of the adopted a-priori profile on the retrieved ClO cannot be neglected, therefore care should be taken when dealing with absolute values. For all MIPAS2D quantities used in this work, data were filtered on the basis of the information gain parameter discussed in Dinelli et al. (2010) and excluding cloud-corrupted spectra. When MIPAS lines of sight crossed optically thick clouds (see next section), information was derived from nearby clear measurements by the tomographic retrieval or lost. Regions of very dense PSC coverage prevented a detailed chemical analysis. For most of the analysis, MIPAS2D data were linearly interpolated onto potential temperature levels calculated from coincident MIPAS2D p and T .

2.3 PSC detection and composition

As discussed, cloud-contaminated spectra are excluded from the GMTR analysis since they can deteriorate the quality of the retrieved parameters. However, the sensitivity of MIPAS to the radiation emitted and scattered by the clouds can be exploited to study PSCs, since MIPAS limb views are sensitive to very optically thin clouds, both during day

and nighttime. PSCs can be detected exploiting the cloud index (CI) technique (Spang et al., 2001). The CI is the ratio of the average spectral radiances in the 788–796 cm⁻¹ range (where gas absorption is dominant) and in the 832–834 cm⁻¹ range (where clouds effects dominate). The ratio is sensitive to the presence of any type of cloud, with lower values associated with increasingly optically thicker clouds. To detect PSCs in MIPAS spectra, we used a CI threshold of 4.5 (Spang and Remedios, 2003) combined with a lower altitude threshold of 16 km to avoid the inclusion of high altitude tropospheric clouds, and an upper altitude limit of 35 km to minimise false detections. In the altitude range from 30 to 35 km, we adopted a more conservative CI = 1.8 in order to avoid false detections (Spang and Remedios, 2003). The 4.5 CI threshold corresponds to a lower detection limit of PSCs with volume density of about 0.2 μm³ cm⁻³ (Höpfner et al., 2006). The tangent altitude of the highest cloudy spectrum in a limb scan was used as an approximated cloud top height (CTH), and the overall PSC analysis is based on CTH measurements. The error on the determined CTH can be assumed to be ± 1.5 km, i.e. about half of the vertical sampling step of MIPAS OR scans or of the vertical projection of the field of view at tangent point (3 km). The CI method has been validated by Höpfner et al. (2009) using the Cloud-Aerosol Lidar and Infrared Pathfinder Satellite Observation (CALIPSO), with MIPAS identifying about 70 % of the PSCs detected by CALIPSO in the Arctic winter.

To determine the PSC composition we applied the empirical methodology developed for MIPAS by Höpfner et al. (2006) on the basis of modelled cloud spectra. The method is based on the NAT spectral signature at 820 cm⁻¹ (Spang and Remedios, 2003) and on the effects due to the large optical depth of ice particles. A new CI (called from now on NAT index) was defined as the ratio between the average intensity over the 819–821 cm⁻¹ spectral range and the average intensity over the 788–796 cm⁻¹ range. Following Höpfner et al. (2006, 2009), PSCs can be classified in three groups based on their composition: ice, NAT and STS/Mix. The classification is performed through a diagram of the color ratio of the NAT index versus the CI index (see Höpfner et al., 2006, Fig. 9). The PSCs classified as ice include mainly PSCs formed by ice particles only. The PSCs classified as NAT are made of at least 30–40 % of NAT particles with mean radius smaller than 3 μm. The PSCs classified as STS/Mix include PSCs which are most likely STS, but can also be of mixed compositions having smaller contributions from NAT or ice. Also PSCs made of very small ice particles or large NAT particles were shown to fall within the last category because of the similarity of their spectral signature to the pure STS case. The STS/Mix should therefore be considered as a mixture of STS, NAT and ice PSCs. Comparison of the PSC composition derived from MIPAS, CALIPSO and lidar by Höpfner et al. (2009) confirmed that the PSCs classified as MIPAS NAT are largely made of non spherical solid particles, the

MIPAS ice are largely made of ice, and MIPAS STS/Mix are mainly a mixture of liquid STS and NAT particles.

2.4 ECMWF meteorological products

In this paper, the vortex edge was identified by using the scaled potential vorticity (sPV, s⁻¹, Manney et al., 1994) derived from the European Centre for Medium-Range Weather Forecasts (ECMWF) high resolution ERA-interim meteorological products. Vortex average quantities were made on the basis of sPV greater than $1.7 \times 10^{-4} \text{ s}^{-1}$. The adopted value is slightly higher than that adopted e.g. by Manney et al. (2006) and allowed a more conservative selection of low in-vortex N₂O values at all potential temperature levels in the stratosphere as compared to lower sPV values. In equipotential maps, the outer and inner vortex edges were shown adopting $\text{sPV} = 1.4 \times 10^{-4} \text{ s}^{-1}$ and $2 \times 10^{-4} \text{ s}^{-1}$. ECMWF sPV values were extracted from the 12 universal time (UT) fields, and could therefore lead to a mismatch between MIPAS observations (performed at fixed local time due to the Sun-synchronous orbit) and the adopted vortex edge. However, a thorough inspection of MIPAS N₂O measurements at the vortex edge showed only minor deviations of the sPV and N₂O tracers, with negligible impact on the calculated vortex averages. We also used ECMWF temperature data in order to assess temperatures associated with detected PSCs.

3 Observation of the 2010–2011 Arctic winter stratosphere

We studied the chemical and physical evolution of the Arctic stratosphere during the 2010–2011 winter by analysing MIPAS measurements in the period from 1 December 2010 to 15 April 2011. The results of the analysis are presented here in terms of averages of the retrieved quantities inside the vortex and, for a few significant cases, also as individual measurements. The results are discussed in Sect. 4.

To show the temporal evolution of the air masses inside the Arctic vortex, Figs. 1 and 2 report MIPAS2D data as vertical distributions of temperature, PSCs and VMRs of N₂O and O₃ (Fig. 1a to d), and of H₂O, HNO₃ and ClONO₂ (Fig. 2a to c). MIPAS2D data shown in the figures were obtained as daily averages within the vortex over isentropes with potential temperature (Θ) ranging between 350 and 1000 K (about 11 to 32 km altitude). Figure 1b reports the detected PSCs (black crosses) plotted over the average temperature of the region having $T < T_{\text{NAT}}$ (hereafter T_{NAT} region). The T_{NAT} temperature is the approximate threshold for PSC formation, and was calculated at each Θ level by applying the formula by Hanson and Mauersberger (1988) to MIPAS2D average H₂O and HNO₃. Figure 2d reports vortex average ClO at Θ = 550 K from am measurements (blue line), at a level where errors were below 100 %. Figure 2d also reports the evolution of the vortex area in terms of fraction of its

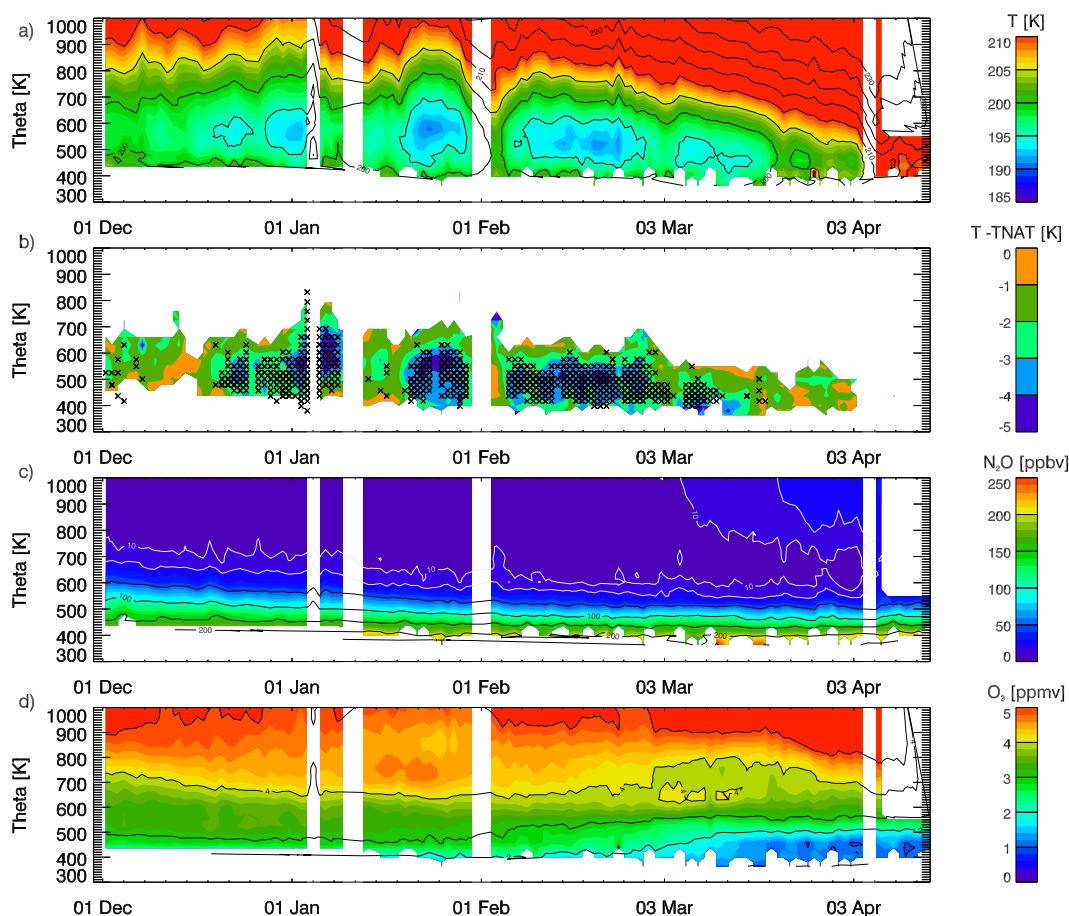


Fig. 1. Time series of MIPAS2D vortex average temperature, T_{NAT} region average temperature, vortex average N_2O and O_3 (top to bottom). The T_{NAT} region temperature in (b) is shown in terms of the difference $T - T_{\text{NAT}}$. (b) also shows the altitude of PSCs detected through MIPAS spectra (black crosses). White vertical regions depict periods with poor or no MIPAS2D data coverage.

maximum extent of $25 \times 10^6 \text{ km}^2$ (black dashed line), and the vortex sunlit daily fraction (red dashed line) both calculated at $\Theta = 550 \text{ K}$.

The geographical behaviour of the vortex was studied by inspecting individual measurements of MIPAS over isentropic surfaces. As an example of the examined data, Fig. 3 reports snapshots at $\Theta = 500 \text{ K}$ of T , N_2O and O_3 , for 3 and 26 February, 8 and 28 March 2011. Similarly, Fig. 4 reports snapshots of HNO_3 , ClONO_2 , and ClO . ClO is reported at 550 K consistently with Fig. 2d. In the two figures, the outer and inner vortex edges (black contour lines) are identified as described in Sect. 2.4. In January and February, the number of measurements contaminated by the presence of PSCs, that are rejected from the analysis, prevented a geographically detailed study at lower Θ values. Only when PSCs disappeared in March could the regions of deepest O_3 depletion around $\Theta = 450 \text{ K}$ be fully observed. The $\Theta = 500 \text{ K}$ level was therefore chosen as a compromise between the Θ level showing the highest ozone depletion (around 450 K) and higher Θ levels having MIPAS spectra less affected by PSCs.

We devote the next sections to the three main aspects characterising the 2010–2011 Arctic winter stratosphere, namely the vortex dynamics, PSC formation and chemical evolution.

3.1 Vortex dynamics

As shown in Figs. 1a and b, during the 2010–2011 winter a well defined and strong vortex led to regions of temperature below T_{NAT} lasting continuously until late March. The vertical extension of these vortex cold regions reached a very wide altitude range in early January, at Θ extending from 430 to 800 K , and then evolved to a progressively lower altitude range, down to Θ from 360 to 550 K in mid-March. Temperature minima dropped persistently below 185 K over limited regions at Θ from 500 to 750 K over 2–7 January, and at Θ from 400 to 650 K over 20–28 January and more sporadically throughout February. The presence of these persistent cold regions is reproduced in the vortex average temperature, displaying a minimum (cold point) below 195 K descending from about $\Theta = 600 \text{ K}$ in early January to 450 K in mid-March (Fig. 1a).

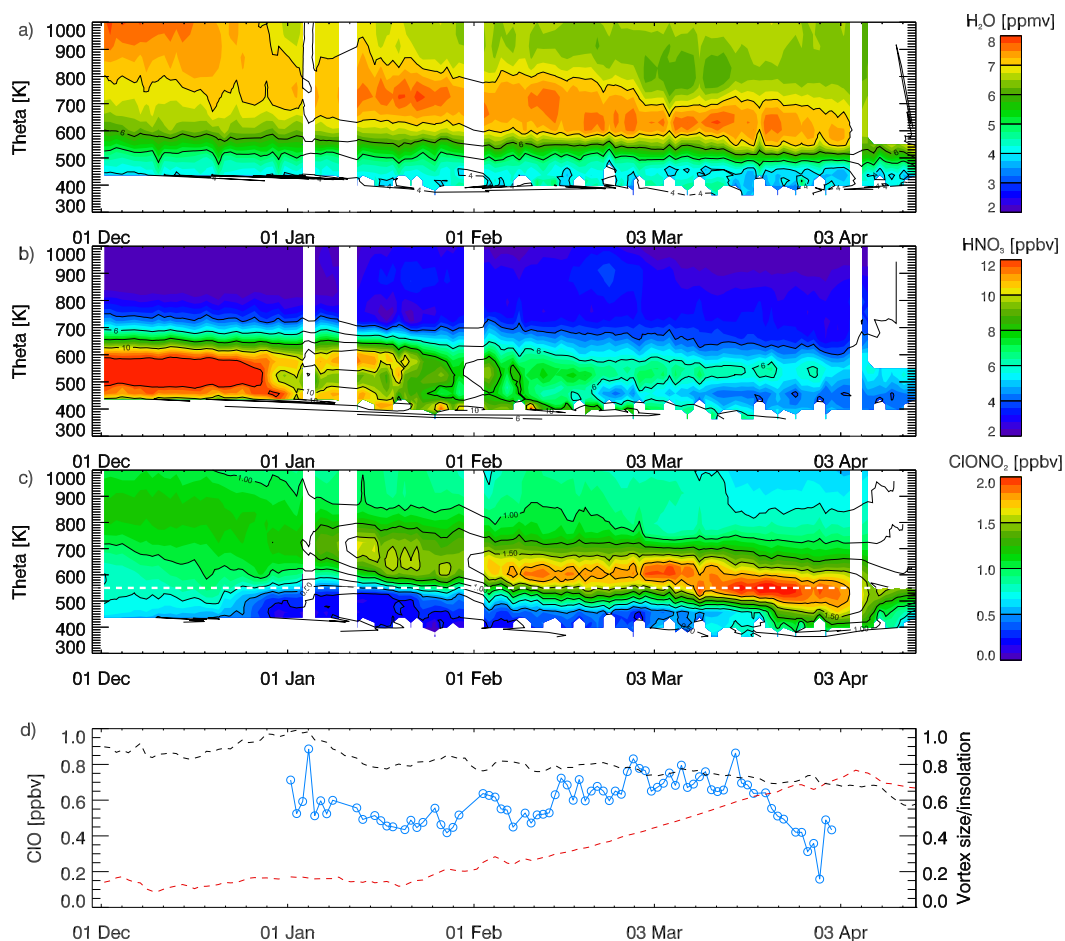


Fig. 2. Time series of MIPAS2D vortex-averaged H_2O , HNO_3 , ClONO_2 and ClO (top to bottom). ClO in **(d)** is shown only as vortex average of am measurements at $\Theta = 550$ K (blue). **(d)** reports also the evolution of the vortex area (black dashed line) in terms of fraction of its maximum extent ($25 \times 10^6 \text{ km}^2$) and the vortex sunlit daily fraction (red dashed line) both calculated at $\Theta = 550$ K (refer to right vertical axis). White vertical regions depict periods with poor or no MIPAS2D data coverage. A white dashed horizontal line at $\Theta = 550$ K was added to the ClONO_2 panel to ease comparison with ClO .

Although the vortex was neither particularly pole-centred nor symmetric (see the events shown in Fig. 3), the vortex size was relatively stable throughout the winter (see the black line in Fig. 2d): beside an expansion and following contraction in late December – early January, the vortex became very slowly smaller in size from December to April (from about 22 down to about $18 \times 10^6 \text{ km}^2$ at Θ from 450 to 550 K). The almost monotonic increase of the sunlit fraction of the vortex implies that the overall displacement of the vortex from the pole was very limited (red line in Fig. 2d). The isolation of the vortex air was well traced by the very low vortex values of N_2O (Fig. 1c) caused by the descent of upper atmospheric air. Vortex N_2O showed signs of mixing with outside vortex air only during a very few time-constrained warming events. The N_2O 100 ppbv isopleth, which will be used in the following sections to trace ozone chemical loss, descended from $\Theta = 550$ down to 450 K from December to April (from

about 21 to 18 km in altitude). The slow diabatic descent was consistently displayed also by H_2O (Fig. 2a).

Occasional planetary wave activity induced a deformation or displacement of the vortex (see Fig. 3), as reflected by the average vortex temperature and N_2O (Fig. 1a to c). For example on 3 February a sudden stratospheric warming (SSW) deformation, induced by a large planetary wave number-two, almost split the vortex into two lobes. This event was accompanied by warmer temperatures in the area where the two lobes were connected, with an indication of mixing with high N_2O values (visible as a peak of N_2O in Fig. 1c). Other relatively less intense events caused an elongation of the vortex followed by ejection of tongues of vortex air towards the extravortex regions, such as those occurring on 8 and 28 March and lasting a few days each (see Fig. 3). During the second event, the inner sPV contour line indicated ejection of air from inner regions of the vortex, resulting in about 10% of vortex air between $\Theta = 400$ and 550 K being ejected. In the

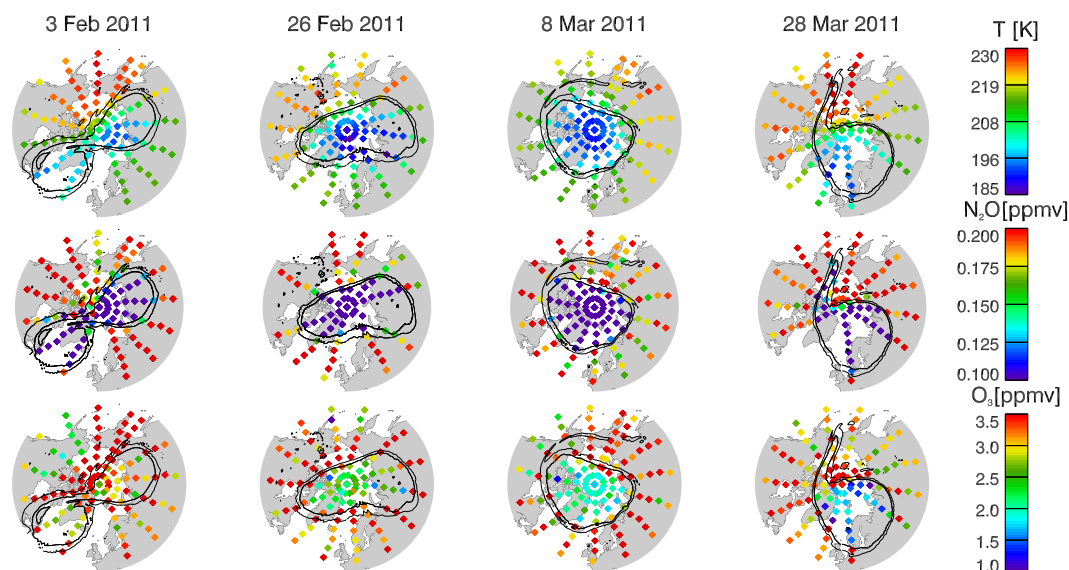


Fig. 3. Snapshots of MIPAS2D temperature, N_2O and O_3 (top to bottom) along MIPAS orbits on the 500 K isentropic surface during selected days in February and March 2011. Only MIPAS am measurements are shown. Black contour lines of constant sPV trace the outer and inner edge of the vortex (respectively with $\text{sPV} = 1.4 \times 10^{-4} \text{ s}^{-1}$ and $2 \times 10^{-4} \text{ s}^{-1}$, thin and thick lines).

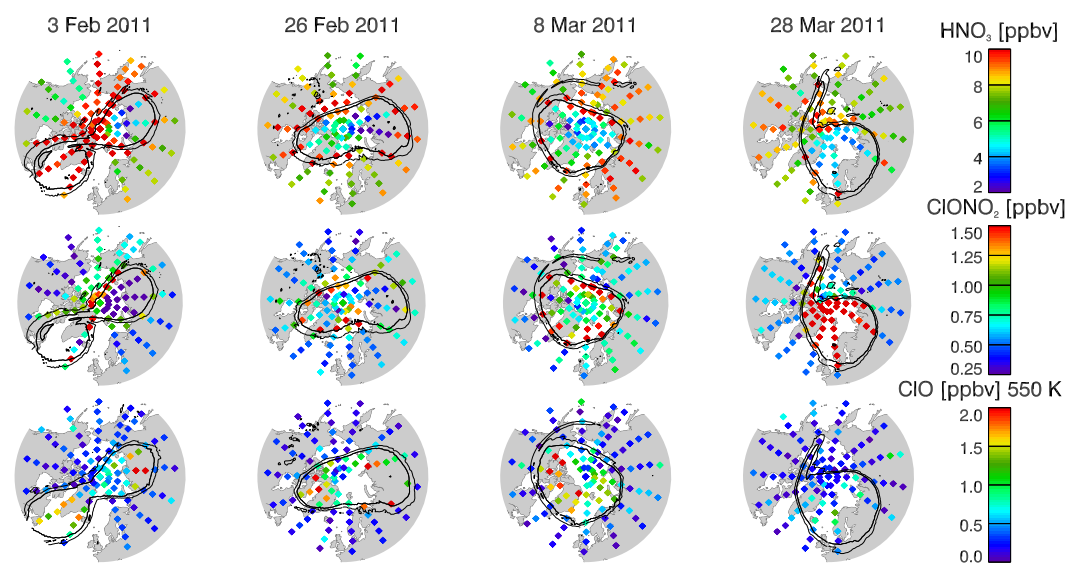


Fig. 4. As in Fig. 3 but for HNO_3 , ClONO_2 , and ClO (top to bottom). ClO is shown on the 550 K isentropic surface (see text for details).

middle stratosphere, events leading to increased N_2O were only marginally reflected in the average temperature (see e.g. late January in Fig. 1a to c). This suggests that these events were sporadic intrusions of outside vortex air with no major impact on the overall vortex isolation. A largely consistent behaviour was found using MIPAS2D CH_4 as passive tracer instead of N_2O , although some differences between the two tracers in early spring will need to be further investigated. Towards early spring, two warmings accompanied the last phases of the evolution of the vortex, which was eventually displaced from the pole on 6 April and persisted as a large

patch of isolated vortex air above Siberia and then Northern Europe until late April. Large concurrent increases in temperature and the N_2O tracer throughout April showed the Arctic return to typical conditions. The final warming was evaluated to be on 19 April 2011 in NCEP-2 reanalysis by Hurwitz et al. (2011).

3.2 Polar stratospheric clouds

The vertical distribution of PSCs detected by MIPAS is reported in Fig. 1b. A total of 3120 MIPAS scans detected

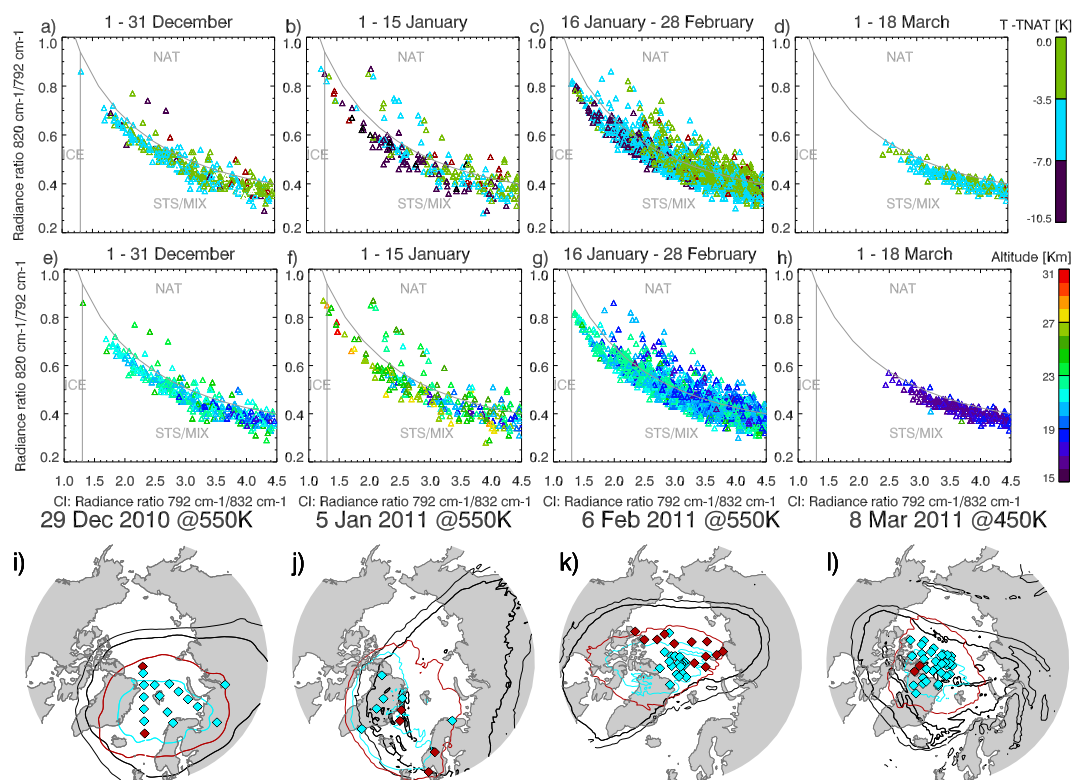


Fig. 5. (a)–(d): Classification of MIPAS detected PSCs in the four periods: 1–31 December 2010, 1–15 January 2011, 16 January–28 February, and 1–18 March, as derived from spectral ratios at the cloud top. Colors indicate the difference between the ECMWF temperature coincident with the detected PSC and the estimated T_{NAT} threshold (red is above T_{NAT}). (e)–(h): as in top panels but with colors indicating PSC altitude. (i)–(l): PSCs classified as NAT (red diamonds) and STS/Mix (cyan diamonds) during selected days of the four periods, together with the regions of predicted PSC occurrence based on ECMWF temperature (red line: NAT region where $T - T_{\text{NAT}} < 0$; cyan line: STS region where $T - T_{\text{NAT}} < -3.5$ K). Vortex edges (black lines) are shown as in Fig. 3.

PSCs over the period 1 December 2010 to 18 March 2011, corresponding to 78 % of days with PSCs out of 97 days of observation. The 2010–2011 Arctic PSC season can be split into four main phases, each having a relatively homogeneous vertical coverage: (i) 1–31 December 2010, with most PSCs occurring at $\Theta = 450$ to 600 K (19–25 km); (ii) 1–15 January 2011, showing an extraordinary vertical coverage up to $\Theta = 700$ K (28 km), with a few individual observations even higher, the highest one at $\Theta = 850$ K (30.5 km); (iii) 16 January–28 February, with the PSCs persistently ranging from $\Theta = 400$ to 600 K (16–24 km); and (iv) 1–18 March 2011, characterised by more sporadic occurrence at $\Theta = 400$ to 500 K (16–19 km). Geographically, the bulk of PSCs clustered close to the cold core of the vortex for most of the winter, following the occasional distortion of the vortex shape.

The results of the analysis of the PSC composition for the four periods, based on the method described by Höpfner et al. (2006) (see Sect. 2.3), are reported in Fig. 5 (panels a–d and e–h). In each color ratio diagram, gray lines delimit the three regions corresponding to PSCs classified as NAT, ice and STS/Mix (see labels in the figure). The color scale in panels a–d represents the difference ($T - T_{\text{NAT}}$) between the tem-

perature coincident with the detected PSC and the estimated T_{NAT} threshold introduced above (red indicates $T > T_{\text{NAT}}$). The color scale in panels e–h corresponds to PSC cloud top height. Since MIPAS measurements contaminated by PSCs were rejected from the retrieval procedure, the temperature assigned to each PSC was taken from ECMWF. Temperatures 3.5 K below T_{NAT} can be considered as a threshold for STS formation (Stein et al., 1999), whereas 7 K below is a prerequisite for the presence of ice (e.g. Weisser et al., 2006, and references therein). Figure 5 also reports snapshots of the geographical distribution of PSCs classified as NAT (red diamonds) or STS/Mix (cyan diamonds) for a selected day from each period (panels i to l). The snapshots also show the regions of expected formation of NAT (red line) and STS (cyan line) PSCs, calculated using ECMWF temperature (with the STS line at $T_{\text{NAT}} - 3.5$ K).

Throughout the season, NAT PSCs were generally warmer as compared to the STS/Mix ones. In general, optically thin clouds (high CI values) were associated with warmer temperatures as compared to optically thick clouds. Besides some scattered PSCs detected in early December (see Fig. 1b), period (i) showed a very compact distribution of PSCs in the

second half of the month. 88 % of PSCs were classified as STS/Mix, 12 % as NAT (Fig. 5a). The temperature associated with each PSC was highly variable, mostly between 5 K below T_{NAT} to above it for a small fraction of PSCs (see color scale in the figure), especially in the case of thinner clouds (high CI values). Although the majority of PSCs were vertically distributed where the average temperature was consistently around the threshold for STS formation (Fig. 1b), temperatures associated with the PSCs of this period were the highest of the 4 periods (compare Fig. 5a–d): the distribution of PSC temperatures peaked just above $T_{\text{NAT}} - 3$ K, pointing to a more likely NAT component, based upon the notion that STS is thought to form only below $T_{\text{NAT}} - 3.5$ K (Stein et al., 1999).

During period (ii), the large vertical spread of the PSC distribution (see Fig. 1b) was reflected in their scattered spectral characteristics (Fig. 5b and f). 79 % of PSCs were classified as STS/Mix, 21 % as NAT and two cases as ice. The bulk of STS/Mix PSCs in the diagram was consistently associated with temperature below STS formation, and was observed between $\Theta = 450$ and 550 K (17–22 km, Fig. 1b and Fig. 5f). At Θ from 550 to 700 K (22–28 km), the STS/Mix PSCs had more scattered color ratio values and associated temperatures often dropped 7 K below T_{NAT} . In a few cases, temperatures reached values above T_{NAT} , suggesting PSC formation within cold mesoscale temperature perturbations that were not reproduced by ECMWF temperatures (e.g. Carslaw et al., 1998) or a mismatch in the temperature association due to very localised cold regions. The large scatter in the color ratio implies very different mixtures in the PSC composition. Two PSCs could be classified as ice based on their spectral signature, and had associated temperatures 7.5 K and 7.0 K below the T_{NAT} threshold (the latter is displayed as cyan in Fig. 5b since it falls in the middle bin of the color scale). These are the only PSCs classified as ice during the whole season, although other ice particles may be present in PSCs classified as STS/Mix. The very high altitude clouds (CTH at $\Theta > 700$ K, 28 km) detected during the very first days of January had an STS/Mix signature extending from the very optically thin region of the diagram (see bottom right of Fig. 5f) towards the ice region in the optically thick part of the diagram (top left of the panel). In some optically thick STS/Mix cases, associated temperatures were above T_{NAT} , as with the lower altitude ones. A detailed investigation of the altitude of the highest PSCs showed that cloud top heights above 30 km were reached by two measurements on 3 January 2011, respectively at 30.2 and 30.5 km altitude above the Eastern coast of Greenland, representing the highest PSCs ever reported in the Arctic. Comparison to synthetic spectra shows that a significant vertical fraction ($> 1/4$) of MIPAS FOV had to be filled by the highest detected PSC, which implies a PSC cloud top height around 30.5 ± 0.75 km. Including the error on MIPAS engineering tangent altitude of 0.5 km leads to a best estimate of 30.5 ± 0.9 km. These extraordinarily high PSCs were confirmed by CALIPSO measurements on

4 January 2011, with PSCs clearly extending above 30 km altitude over the same region (see http://www-calipso.larc.nasa.gov/products/lidar/browse_images/show_calendar.php).

In period (iii), the bulk of PSCs persisted at $\Theta = 500$ –600 K (20–24 km) (Fig. 5c). 82 % of PSCs were classified as STS/Mix, and 18 % as NAT. Consistent with a predominant STS composition, most PSCs falling in the STS/Mix portion of the diagram have an associated temperature 3 to 7 K below T_{NAT} , with the PSC temperature distribution peaking below 5 K (the coldest of the season). Comparison to vortex averaged temperature (Fig. 1a) shows that PSCs occurred only where a large fraction of the vortex was colder than T_{NAT} . This suggests that these PSCs were optically thick clouds associated with synoptic scale temperature (Adriani et al., 2004), a characteristic that is consistent with the stable and continuous cold temperatures observed throughout February. During period (iv), PSCs were observed until 18 March and only around $\Theta = 400$ –500 K (16–19 km, Fig. 1b). 94 % of these late PSCs were classified as STS/Mix, whereas only 6 % as NAT, and they were largely optically thinner than in the previous periods. The associated temperature also supports the STS/Mix composition.

A comparison of the location of the classified PSCs with NAT and STS regions predicted from ECMWF temperature showed overall good agreement. Although not representative of the whole PSC population, Fig. 5i–l report some events with good consistency between the classified PSC and the expected NAT and STS regions, tracking their very inhomogeneous geographical distributions. This points to a generally acceptable assignment of the PSC composition. Some inconsistencies for individual cases are due to PSCs being at the edge of the finite altitude and temperature thresholds adopted for the figures. Following Höpfner et al. (2006, 2009), and as pointed out in Sect. 2.3, the NAT classification implies that the spectral signature of NAT particles was strong. This means that each of the PSCs we classified as NAT was composed of at least 30–40 % of such particles with mean radii smaller than 3 μm . In contrast, the STS/Mix class indicates the presence of clouds which contain STS droplets, large NAT particles, or mixtures of the two. Since large NAT particles (3–6 μm) lead to very similar spectral signatures as STS, the STS/Mix class cannot rule out the possibility of having large NAT particles (or even NAT rocks, Fahey et al., 2001) in the corresponding cases. The presence of a fraction of observed clouds composed of STS droplets is suggested by the fact that coincident temperatures were largely below the STS formation threshold. The overall fraction of 17 % of NAT classified PSCs in the 2010–2011 Arctic winter can be therefore considered a good estimate of PSCs with dominant NAT composition.

3.3 Chemical evolution of the Arctic

3.3.1 HNO₃ and H₂O

As a result of PSC formation and subsequent sedimentation of PSC particles, HNO₃ was significantly removed from the lower stratosphere from January to April (Fig. 2b). Vortex HNO₃ decreased from 10 to 4 ppbv within the isentropic range $\Theta = 450\text{--}550$ K, down to $\Theta = 400\text{--}500$ K late in the season, roughly following the descending N₂O 100 ppbv isopleth. In this layer PSCs were almost continuously detected. In particular, the relatively higher vortex averaged HNO₃ following the SSW on 3 February was promptly depleted by the subsequent persistent PSC formation, with a 50% drop in about a month (Fig. 2b). The layer descending from about $\Theta = 600$ K to $\Theta = 500$ K had a relatively weaker reduction in HNO₃. During most of the winter, the lowest amounts of HNO₃ were found within or close to the cold core of the vortex, where the bulk of PSCs occurred (Fig. 4, top row). The low HNO₃ occurred where temperatures were below the STS formation threshold, suggesting capture by STS/Mix PSCs (see Sect. 3.1). On some occasions, strips of NAT PSCs were clearly coincident with the deepest minima of HNO₃. Since the HNO₃ did not recover when the PSC season ended in mid-March, denitrification must have occurred permanently. The observed low HNO₃ values can be therefore associated with both temporary sequestration by STS/Mix PSCs and denitrification associated with PSCs composed of large NAT particles. Removal of HNO₃ at $\Theta = 450\text{--}500$ K was accompanied by sporadic increases of HNO₃ and NO₂ (not shown) at $\Theta = 400\text{--}450$ K, likely as a result of evaporation of sedimenting particles at lower levels. As expected by the lack of ice PSCs, H₂O (Fig. 2a) showed only a marginal decrease in late March in the lower stratosphere. As mentioned in Sect. 3.1 the overall trend in H₂O was consistent with the diabatic descent.

3.3.2 ClONO₂ and ClO

ClONO₂ was greatly depleted in the lower stratosphere at $\Theta = 400\text{--}550$ K (Fig. 2c) in January and February, then followed by a recovery in March. The largest depletion was coincident with the beginning of the marked decrease in HNO₃ starting in late December. The very low ClONO₂ in January extended throughout the inner vortex, and was accompanied by a collar of high values at the vortex edge (Fig. 4, middle row). The low ClONO₂ during February was accompanied by activation of ClO in the vortex, reaching a maximum in mid-March (see time series at $\Theta = 550$ K in Fig. 2d). This is also shown by ClO maps (Fig. 4, bottom row), with sporadic high ClO values progressively increasing from the more isolated outer regions of the vortex in February to being more homogeneously distributed in March. Even then, ClO continued to be higher outside the centre of the vortex, most likely because the core of the vortex remained largely in darkness in

early March (only about 60% of the vortex was sunlit in mid-March, see Fig. 2d). Around 18 March, when the last PSCs disappeared, vortex-average ClO started to dramatically decrease, accompanied by an analogous prompt increase in ClONO₂. At this late stage, ClONO₂ recovered throughout the vortex while patches of high ClO persisted in scattered regions of the vortex until early April.

3.3.3 O₃

As a consequence of chlorine activation, Arctic vortex O₃ in 2011 was greatly depleted in the lower stratosphere at $\Theta = 400\text{--}500$ K (see Fig. 1d). At $\Theta = 450$ K, vortex average O₃ dropped from 3 ppmv in early January to 0.95 ppmv in early April. Daily depletion rates reached 100 ppbv day⁻¹ in mid-March. A second region of minimum was reached in the middle stratosphere at $\Theta = 700\text{--}800$ K, with average O₃ decreasing from 4.5 ppmv in mid-January down to 3 ppmv in mid-March. The intermediate layer around $\Theta = 600$ K showed little change in O₃. The meteorology of the 2011 Arctic vortex with the PSC season extending up to mid March played a key role in the lower stratospheric depletion (see Fig. 1b and d). Snapshots on the 500 K isentrope (about 20 km altitude) reported in Fig. 3c show depletion of O₃ occurring within the vortex since January with scattered low values in progressively larger areas of the vortex. O₃ depletion in February and March tended to be more pronounced in the outer parts of the vortex (see 28 March snapshot in Fig. 3), with occasional perturbations of the vortex causing a mixing with higher vortex values and leading to a more homogeneous distribution (see 8 March snapshot). The O₃ chemical loss was evaluated taking into account the descent of the N₂O 100 ppbv isopleth observed in Fig. 1c (Proffitt et al., 1990; Rex et al., 2002). Comparison of the minimum value of 0.95 ppmv reached by vortex averaged O₃ at $\Theta = 450$ K in early April to the 3.4 ppmv of O₃ at $\Theta = 550$ K in December following the evolution of the N₂O 100 ppbv isopleth (see Sect. 3.1) results in an estimate of the chemistry-driven depletion of vortex O₃ of about 70% at this level.

3.3.4 Measurement of total depletion of O₃ and HNO₃

The diagnostics adopted for this study involved interpolation to Θ levels. The interpolation may introduce a smoothing error in the vertical profiles, artificially removing sharp changes in the vertical gradient of the retrieved quantity. We therefore further investigated the occurrence of low O₃ and HNO₃ values in the original data retrieved on the fixed altitude grid (with relevant grid points at 15, 18 and 21 km – see Sect. 2). Figure 6a and c show time series of individual O₃ and HNO₃ VMR at the 18 km altitude grid point, both for vortex (blue) and outside vortex (gray) data North of 65° N. In March and early April, the 18 km altitude within the vortex corresponds to $\Theta = 460 \pm 12$ K, whereas $\Theta = 450$ K corresponds to an altitude of 17.8 ± 0.5 km. The difference in

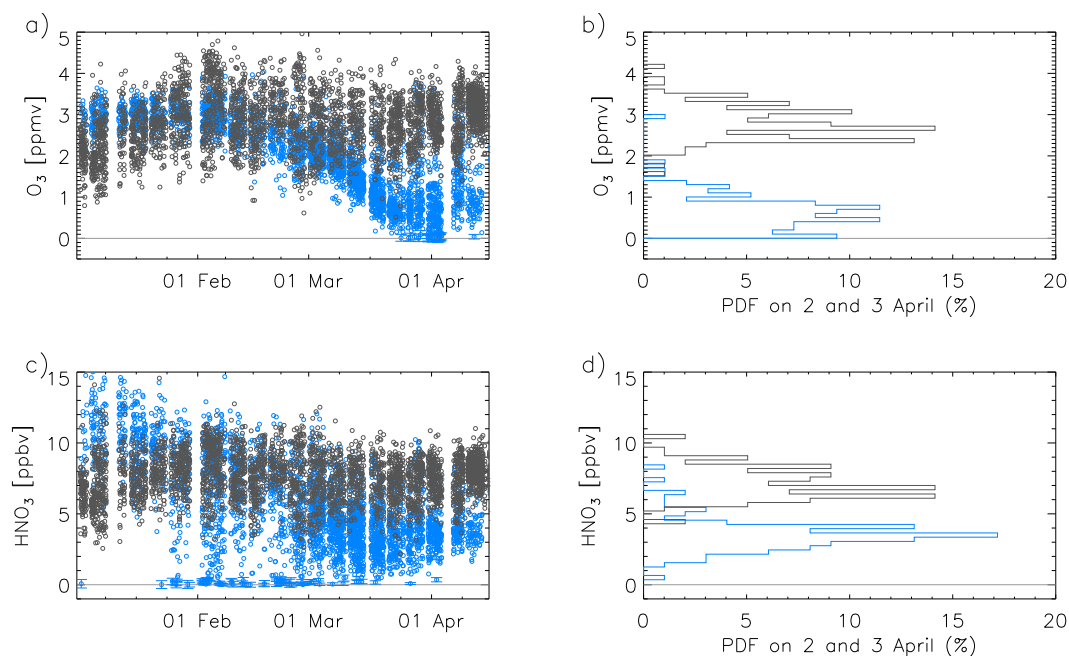


Fig. 6. Time series (left) and probability distribution functions (PDFs) on 2–3 April 2011 (right) of MIPAS2D individual measurements of O_3 (top) and HNO_3 (bottom) at the 18 km retrieval grid point and North of 65° geographical latitude. Vortex (blue) and outside vortex (gray) data are shown. In the time series panels (left), error bars are shown only for measurements close to zero.

altitude falls therefore below the 3–4 km vertical resolution of the retrieved data. The O_3 time series show a progressively larger divergence between vortex and outside vortex values as the season evolved. While the distribution of vortex O_3 values at 18 km altitude was very compact until late March, in early April it displayed a much broader spread. This shows that O_3 started to recover in some parts of the vortex while it was reaching its deepest depletion in other parts. O_3 reached 100 % depletion in a fraction of the vortex in late March and early April. Figure 6 reports also the corresponding probability distribution functions (PDFs) calculated over 2 and 3 April. Vortex O_3 in early April had a relatively flat distribution of VMR values extending from 0 to 1 ppmv. About 10 % of the vortex measurements at 18 km altitude are consistent with total depletion of O_3 within the measurement random error of around 0.1 ppmv. The average vortex ozone at 18 km altitude dropped to 0.6 ppmv in 2–3 April. If compared to the average vortex O_3 in December at 21 km altitude grid point (i.e. along the 100 ppbv N_2O isopleth as discussed in the previous section), the drop corresponds to 80 % O_3 depletion.

Analogously, Fig. 6c shows the clear inhomogeneity in HNO_3 . Loss of HNO_3 had the largest effect on parts of the vortex in late January and February, with greatly scattered low values, especially after the SSW on 3 February. Low vortex HNO_3 was then more homogeneously distributed in March and early April (Fig. 6c and d). The severe depletion of HNO_3 in certain parts of the vortex halted in early March in accordance with PSCs disappearing. Both for O_3

and HNO_3 , error bars are shown for close to zero values to highlight their accuracy.

4 Discussion

4.1 Comparison to previous Arctic winters

The behaviour of the 2010–2011 Arctic winter stratosphere was compared to Arctic winters observed during MIPAS mission from 2003 to 2010. Figure 7 reports time series of daily vortex averages of selected targets (see labels) at $\Theta = 450$ K for individual years 2011 (blue line with circles) and 2003 to 2010 (gray circles). The 2003–2010 multi-year average is shown as a thick gray line. Since in many past Arctic winters the vortex disappeared before spring, it should be noted that the distribution in time of the multi-year average at a certain date is given by only those years for which the Arctic vortex was defined. The figure also reports, for selected targets, the average over the reference T_{NAT} region (green) introduced in Sect. 3.

The 2010–2011 Arctic winter stratosphere was close to 2003–2010 values for most targets until mid-January. It then entered the period of remarkably stable cold temperatures discussed in the previous section, and started to significantly differ from the distributions of values observed in previous years. Temperatures in February through March remained at 10 to 20 K below the multi-year average of previous MIPAS-observed years (Fig. 7a), with a cold core of the vortex traced

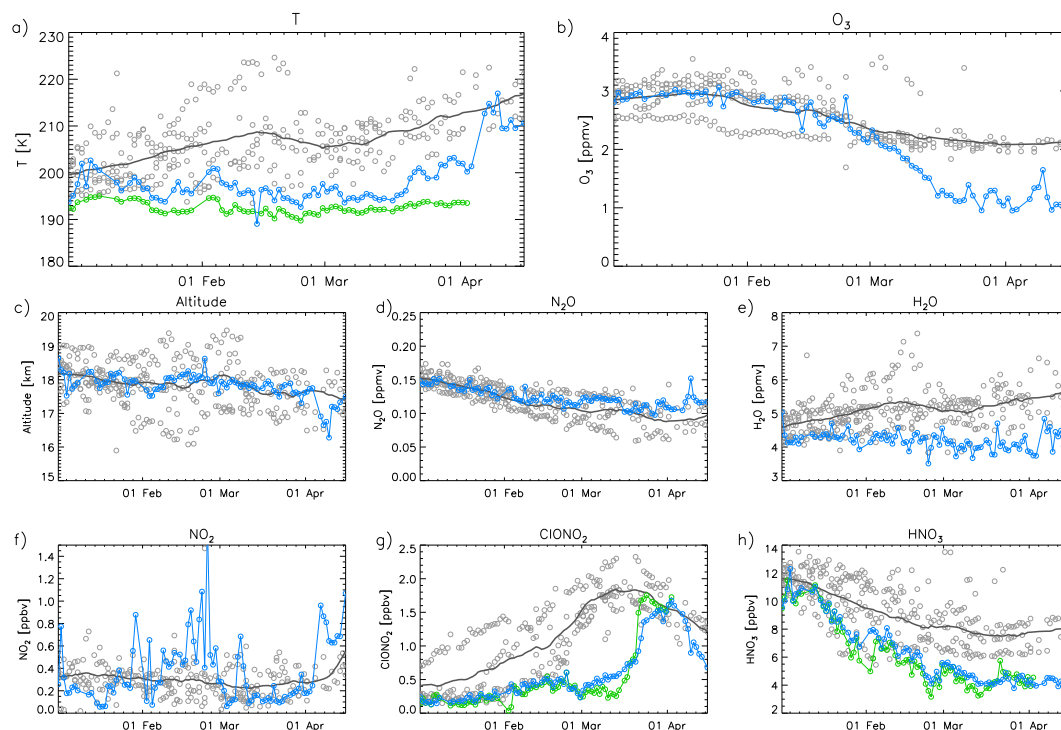


Fig. 7. Time series of daily vortex-averaged MIPAS2D targets on the 450 K isentrope during January to April for individual years 2003 to 2010 (gray circles) and 2011 (blue). The 2003–2010 multi-year mean is shown as a thick gray line. MIPAS2D 2011 data averaged within the T_{NAT} region (green) are also shown. Targets are temperature and O₃ (top panels), altitude of retrieved data, N₂O and H₂O (middle panels), NO₂, ClONO₂ and HNO₃ (bottom panels).

by the T_{NAT} region persisting until early April. The altitude of the 450 K isentrope was remarkably close to the average of the previous years, corresponding to about 18 km altitude throughout the winter (Fig. 7c), and about 55 hPa. The 2011 N₂O displayed values more constant in time (Fig. 7d), pointing to a slower diabatic descent. The slower descent is also shown by H₂O which was about 20 % below the multi-year average (Fig. 7e), opposite to the ascending trend in H₂O observed in typical years.

In terms of PSCs, the 2010–2011 PSC season extended until mid-March, 2 to 4 weeks longer than in other recent cold winters (e.g. Pitts et al., 2011). The altitude range covered by PSCs during 2010–2011 Arctic winter was also anomalous, with PSCs reaching altitudes around 30 km, as compared to maximum altitudes of 26–28 km previously observed (e.g. Poole and Pitts, 1994; Fromm et al., 1999; Massoli et al., 2006). The observed fraction of 17 % of predominantly NAT PSCs is very close to the 14 % of NAT-only PSCs found by Maturilli et al. (2005) over 1995–2003 using ground based lidar observations.

Nitric acid in the 2011 lower stratosphere was about 40 % lower than the 2003–2010 multi-year average. It remained low also when temperatures rose at the end of March as a consequence of denitrification (Fig. 7h). Comparison of the HNO₃ averaged over the T_{NAT} region and over the vortex as a

whole show that denitrification was stronger within the cold core, consistent with the PSC distribution. NO₂ at $\Theta = 450$ K (Fig. 7f) showed sporadic very high values, more often than previous years. In particular, the highest NO₂ values were reached in the last few days of January and in the last week of February consistent with two periods of minimum HNO₃. In both cases, the high NO₂–low HNO₃ values were coincident with a reduction in the PSC distribution following prolonged periods of PSC occurrence. Whether this is associated with release of nitrogen following temporary capture by low altitude PSCs has to be further investigated. ClONO₂ was close to some previous years until mid-February, then remained significantly depleted (Fig. 7i). The drop in late February to mid-March was coincident with the period of highest ClO (see Fig. 2d), which reached its peak value on 15 March. ClO then started to be converted into its reservoirs, as shown by the prompt increase of ClONO₂, reaching previous years' values (compare averages at $\Theta = 550$ K in Fig. 2c and d). In particular, an abrupt change in ClONO₂ occurred in the colder part of the vortex (see green curve in Fig. 7i), with a slower change in the vortex average due to already high values in the outer part of the vortex (see Fig. 4). This prompt ClONO₂ change points to reconversion of ClO mainly into the ClONO₂ reservoir. Comparison to results by Manney et al. (2011, their Fig. 2) shows that over

the third week of March ClO reconverted to reservoir partitioning, with about 60–75 % going into ClONO₂ and about 40–25 % into HCl. Therefore chlorine deactivated partially into HCl, which is anomalous for Arctic winters, although a detailed modelling of the processes will be necessary to draw a firmer conclusion. The deactivation of ClO stabilised O₃ around 1 ppmv below the range of 2003–2010 average for almost a further month. As discussed in Sect. 3.3.3, also in the middle stratosphere ($\Theta = 700\text{--}800\text{ K}$) O₃ was severely depleted by 25 % down to 3.3 ppmv (see Fig. 1), matching the lower edge of the 2003–2010 range (not shown).

The most dramatic difference with previous years was however observed in O₃, showing a compact trend that reached values below average only in March (Fig. 7b). With PSCs continuing to form until 18 March at this Θ level, O₃ depletion continued until early April, down to about 50 % of typical values from previous years.

Previous major Arctic ozone depletions occurred in winters 1995–1996 (Manney et al., 1996), 1999–2000 (Rex et al., 2002; Feng et al., 2005) and 2004–2005 (Manney et al., 2006; Rex et al., 2006). Adding 2010–2011 to the list, the severity of these major ozone losses has been increasing over time. In all of the previous winters, the season of cold temperatures has in fact persisted for a shorter period and was halted earlier than in 2011. Only in 1996–1997 did cold temperatures last until March, although the ozone depletion was limited because of a warmer early winter (Newman et al., 1997). The longer 2011 PSC season and the delayed re-conversion of ClO into its reservoirs caused the 2011 daily O₃ depletion rate to reach 100 ppbv day⁻¹, as compared to the 40 ppbv day⁻¹ in the previous record depletion in 2005 (Rex et al., 2006). Considering the maximum O₃ daily depletion rate reached in mid-March, complete O₃ destruction at $\Theta = 450\text{ K}$ would have likely occurred in 2011 with only a further week of active chlorine cycles. Given the more prolonged PSC coverage of 2011, this different behaviour is in line with the linear relationship between the total O₃ depletion and V_{PSC} integrated over the winter (Harris et al., 2010). The observed 2011 denitrification had a greater role than in previous years (see also Manney et al., 2011), with regions of complete removal of HNO₃ accompanying detection of STS/Mix and NAT PSCs. Although NAT PSCs made of large particles could not be excluded, the much larger fraction of STS/Mix PSCs observed confirms their active contribution in driving the Arctic lower stratospheric chemistry (WMO, 2011). If we also consider the O₃ minima reached in the middle stratosphere ($\Theta = 700\text{--}800\text{ K}$), 2011 showed both a very large NO_x driven ozone depletion above $\Theta = 650\text{ K}$ as occurred in 2007 (due to the persistent isolation of the upper vortex) and the largest PSC-ClO driven depletion in the lower layers (for example, see Kuttippurath et al., 2010).

4.2 Comparison to Antarctic conditions

The above picture is remarkably close to the conditions typically observed over the Antarctic. An inter-hemispheric comparison of conditions in the Northern polar region to typical conditions in the Southern polar region during the respective winters is presented in Fig. 8. The figure shows monthly mean vertical profiles of MIPAS2D target quantities in the Arctic (blue line with circles for March 2011 and gray lines for the same month in 2003 to 2010), and in the Antarctic (red line with circles for September 2008). March and September have approximately seasonally symmetric conditions in the two hemispheres. Averages were performed on pressure levels and respectively over the 75°–90° N and 75°–90° S geographical latitude, so as to reflect both chemical and dynamical changes of the vortex. In addition to temperature and O₃ (Fig. 8, top panels), the figure reports the same targets discussed in the previous section (see labels in the figure). In terms of temperature, altitude, N₂O and H₂O tracers (Fig. 8a, c, d and e), the 2011 Arctic conditions are closer to the Antarctic conditions than to 2003–2010 Arctic winters. The average temperature profile in 2011 resembled the clear vertical *S* shape found in the Antarctic with well defined temperature cold point and stratopause, in contrast to many Arctic winters showing a dynamically-driven almost isothermal lower stratosphere. 2011 N₂O traced a strong isolation of the vortex down to roughly 20 hPa in agreement with the Antarctic N₂O profile. The similarity in the dynamical conditions of the 2011 Arctic and 2008 Antarctic are reflected also in the H₂O profiles. The only Arctic year displaying N₂O and H₂O profiles close to 2011 was 2007 (dashed gray line). Both in the 2011 Arctic and 2008 Antarctic, the altitude of constant pressure surfaces at latitude >75° between 50 and 2 hPa (about 18 and 40 km altitude) was up to 10 % lower than average Arctic conditions.

Despite very similar dynamical conditions, Arctic O₃ reduction in 2011 was less pronounced than in the Antarctic, consistent with much weaker denitrification (Figs. 8b and e). At 20 to 10 hPa (which corresponds to $\Theta = 650\text{--}800\text{ K}$ in the middle stratosphere discussed above) most Arctic parameters (at 10 hPa for O₃) are close to Antarctic conditions, although with a different partitioning of the nitrogen family (see NO₂, ClONO₂ and HNO₃ in Fig. 8f to h). In the lower stratosphere, also the 2011 Arctic winter ClO was deactivated into ClONO₂, but to a lesser extent as compared to previous Arctic winters both due to the late deactivation of ClO and a partial partitioning into HCl. ClONO₂ reached higher values in March as compared to Antarctic conditions (Fig. 8g) where ClO deactivates through HCl: This implies that although 2011 conditions were closer to the Antarctic than ever before, also 2011 maintained ClONO₂ as the main pathway for ClO deactivation (together with HCl to a lesser extent). This is in agreement with HCl becoming the dominant reservoir when vortex O₃ drops below 0.5 ppmv as typically reached in the Antarctic (Santee et al., 2008, and

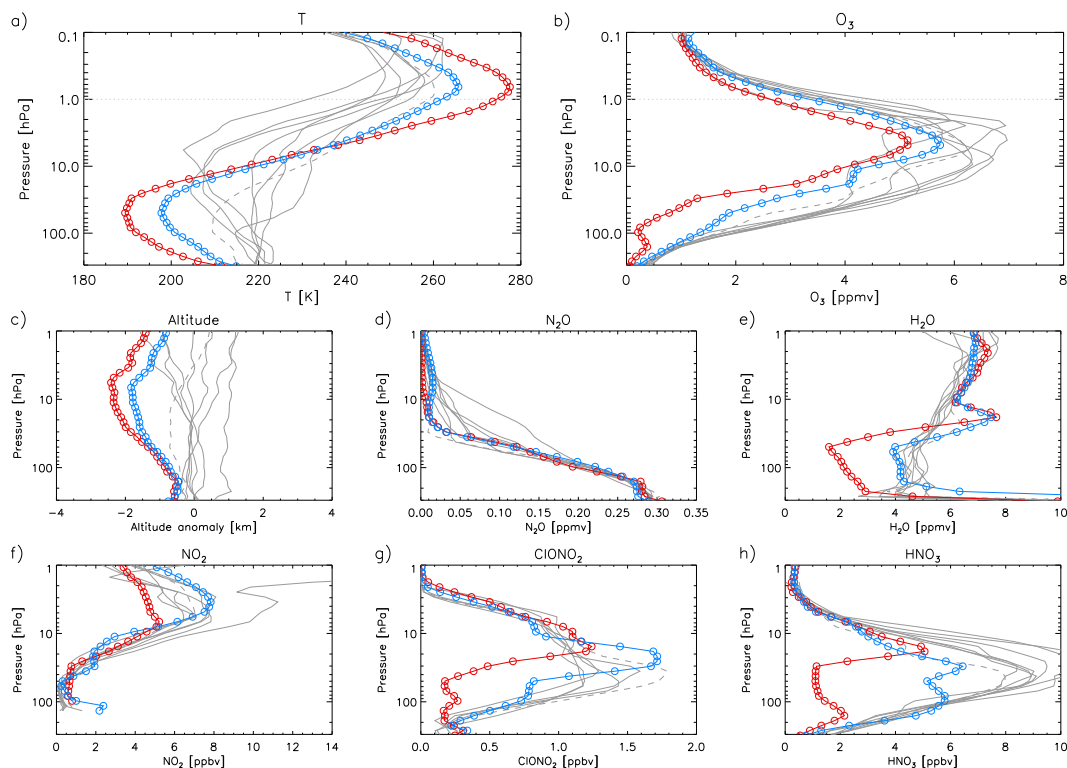


Fig. 8. MIPAS2D monthly mean vertical profiles for selected targets in the Arctic for March 2011 (blue line with circles) and 2003 to 2010 (gray lines; 2007 dashed), and in the Antarctic for September 2008 (red line with circles). Data are averaged poleward of 75° geographical latitude. Targets are temperature and O_3 (top panels), altitude of retrieved data, N_2O and H_2O (middle panels), NO_2 , ClONO_2 and HNO_3 (bottom panels). The altitude is shown as difference from the 2003–2010 Arctic average. Note that profiles extend from 300 to 1 hPa, apart from temperature and O_3 , which extend up to 0.1 hPa.

references therein). These values of O_3 were only marginally observed in the 2011 Arctic.

5 Conclusions

We presented MIPAS/ENVISAT observations of 2010–2011 Arctic winter retrieved with a 2-D tomographic approach. The 2010–2011 Arctic winter was characterised by a stronger than usual late vortex with persistent cold temperature, and a PSC season extending until mid-March. In the lower stratosphere, this led to a progressively stronger O_3 depletion correlated with active ClO, until sublimation of PSCs restored the ClONO_2 reservoir almost a month later than in typical years. In early April, 10 % of vortex O_3 measurements at the 18 km retrieval altitude (about $\Theta = 460$ K) were consistent with total depletion and vortex average O_3 reached 0.6 ppmv. This corresponds to an 80 % chemical loss from the beginning of the winter along the descending 100 ppbv N_2O isopleth. In early January, the detected PSCs reached altitudes above 30 km previously unreported in the Arctic region. About 17 % of the PSCs were classified as NAT, while 83 % of PSCs were STS/Mix, pointing to their major role in driving the Arctic chemistry. As compared to

2003–2010 average values, vortex O_3 was lower by 50 % at $\Theta = 450$ K and by 35 % at 550 K in March. In the middle stratosphere ($\Theta = 700$ – 850 K) O_3 was depleted by 25 % down to 3.3 ppmv, at the lower edge of the 2003–2010 range. 2011 showed the largest ozone depletion ever reported in the Arctic stratosphere.

Our results are largely in agreement with the analysis of the 2010–2011 winter recently published by Manney et al. (2011) and by Sinnhuber et al. (2011), which showed that close-to ozone hole conditions were reached in the 2011 Arctic. In particular, the lowest vortex average O_3 of 0.6 ppmv which we observed in early April was missed by the Microwave Limb Sounder (MLS) adopted by Manney et al. (2011) due to instrumental shut down, but confirmed by two soundings they report for $\Theta = 465$ K (their Fig. 4c). Comparison of our ClONO_2 to their HCl trends suggests 2011 Arctic ClO deactivated into ClONO_2 as a main pathway, and to a lesser extent into HCl (which did not show the same prompt increase). Our results are also in agreement with those by Sinnhuber et al. (2011), with a difference in their minimum 0.3 ppmv value reached by individual ozone measurements at 18 km altitude, against our 10 % of vortex O_3 values being consistent with total depletion. Both results are compatible

within the given random errors (about 0.1–0.15 ppmv), although biases between the different retrievals are under investigation.

2011 Arctic conditions were remarkably closer to those observed in the Antarctic than ever before, although they maintained some distinct peculiarities of Arctic winters both in chlorine partitioning and in the composition of PSCs. The adopted MIPAS2D approach showed a good reproduction of vortex patchy features or filaments through the N₂O tracer, therefore pointing to a similar benefit for active targets. This further motivates the exploitation of the 2-D approach for future studies when dealing with scattered low values within the Arctic vortex or ejections of vortex air towards middle latitudes.

Acknowledgements. The authors are grateful to A. Dudhia who first pointed them towards the extreme conditions of the 2010–2011 Arctic winter. The authors are grateful to S. Viscardi and Q. Errera for providing the meteorological data and guidance on how to use them. E. A. and E. P. acknowledge the support by ESA within the framework of the Changing Earth Science Network Initiative. The authors wish to thank the anonymous reviewers and the editor for their comments and suggestions, which greatly improved the quality of the paper.

Edited by: M. von Hobe

References

- Adriani, A., Massoli, P., Di Donfrancesco, G., Cairo, F., Moriconi, M. L., and Snels, M.: Climatology of polar stratospheric clouds based on lidar observations from 1993 to 2001 over McMurdo Station, Antarctica, *J. Geophys. Res. Atmos.*, 109, D24211, doi:10.1029/2004JD004800, 2004.
- Andrews, D. G., Holton, J. R., and Leovy, C. B.: Middle atmosphere dynamics, 1st Edition, Academic Press, New York, NY, USA, 1987.
- Carlotti, M., Dinelli, B. M., Raspollini, P., and Ridolfi, M.: Geo-fit Approach to the Analysis of Limb-Scanning Satellite Measurements, *Appl. Optics*, 40, 1872–1885, doi:10.1364/AO.40.001872, 2001.
- Carlotti, M., Brizzi, G., Papandrea, E., Prevedelli, M., Ridolfi, M., Dinelli, B. M., and Magnani, L.: GMTR: Two-dimensional geo-fit multitarget retrieval model for Michelson Interferometer for Passive Atmospheric Sounding/Environmental Satellite observations, *Appl. Optics*, 45, 716–727, doi:10.1364/AO.45.000716, 2006.
- Carslaw, K. S., Wirth, M., Tsias, A., Luo, B. P., Dörnbrack, A., Leutbecher, M., Volkert, H., Renger, W., Bachmeister, J. T., and Peter, T.: Particle microphysics and chemistry in remotely observed mountain polar stratospheric clouds, *J. Geophys. Res.*, 103, 5785–5796, doi:10.1029/97JD03626, 1998.
- Dinelli, B. M., Alpaslan, D., Carlotti, M., Magnani, L., and Ridolfi, M.: Multi-target retrieval (MTR): the simultaneous retrieval of pressure, temperature and volume mixing ratio profiles from limb-scanning atmospheric measurements, *J. Quant. Spectrosc. Radiat. Transfer*, 84, 141–157, doi:10.1016/S0022-4073(03)00137-7, 2004.
- Dinelli, B. M., Arnone, E., Brizzi, G., Carlotti, M., Castelli, E., Magnani, L., Papandrea, E., Prevedelli, M., and Ridolfi, M.: The MIPAS2D database of MIPAS/ENVISAT measurements retrieved with a multi-target 2-dimensional tomographic approach, *Atmos. Meas. Tech.*, 3, 355–374, doi:10.5194/amt-3-355-2010, 2010.
- Fahey, D. W., Gao, R. S., Carslaw, K. S., Kettleborough, J., Popp, P. J., Northway, M. J., Holecek, J. C., Ciciora, S. C., McLaughlin, R. J., Thompson, T. L., Winkler, R. H., Baumgardner, D. G., Gandrud, B., Wennberg, P. O., Dhaniyala, S., McKinney, K., Peter, T., Salawitch, R. J., Bui, T. P., Elkins, J. W., Webster, C. R., Atlas, E. L., Jost, H., Wilson, J. C., Herman, R. L., Kleinböhl, A., and von König, M.: The Detection of Large HNO₃-Containing Particles in the Winter Arctic Stratosphere, *Science*, 291, 1026–1031, doi:10.1126/science.1057265, 2001.
- Farman, J. C., Gardiner, B. G., and Shanklin, J. D.: Large losses of total ozone in Antarctica reveal seasonal ClO_x/NO_x interaction, *Nature*, 315, 207–210, doi:10.1038/315207a0, 1985.
- Feng, W., Chipperfield, M. P., Davies, S., Sen, B., Toon, G., Blavier, J. F., Webster, C. R., Volk, C. M., Ulanovsky, A., Ravegnani, F., von der Gathen, P., Jost, H., Richard, E. C., and Claude, H.: Three-dimensional model study of the Arctic ozone loss in 2002/2003 and comparison with 1999/2000 and 2003/2004, *Atmos. Chem. Phys.*, 5, 139–152, doi:10.5194/acp-5-139-2005, 2005.
- Fischer, H., Birk, M., Blom, C., Carli, B., Carlotti, M., von Clarmann, T., Delbouille, L., Dudhia, A., Ehhalt, D., Endemann, M., Flaud, J. M., Gessner, R., Kleinert, A., Koopman, R., Langen, J., López-Puertas, M., Mosner, P., Nett, H., Oelhaf, H., Perron, G., Remedios, J., Ridolfi, M., Stiller, G., and Zander, R.: MIPAS: an instrument for atmospheric and climate research, *Atmos. Chem. Phys.*, 8, 2151–2188, doi:10.5194/acp-8-2151-2008, 2008.
- Fromm, M. D., Bevilacqua, R. M., Hornstein, J., Shettle, E., Hopfel, K., and Lumpe, J. D.: An analysis of Polar Ozone and Aerosol Measurement (POAM) II Arctic polar stratospheric cloud observations, 1993–1996, *J. Geophys. Res.*, 1042, 24341–24358, doi:10.1029/1999JD900273, 1999.
- Glatthor, N., von Clarmann, T., Fischer, H., Grabowski, U., Höpfner, M., Kellmann, S., Kiefer, M., Linden, A., Milz, M., Steck, T., Stiller, G. P., Mengistu Tsidu, G., Wang, D.-Y., and Funke, B.: Spaceborne ClO observations by the Michelson Interferometer for Passive Atmospheric Sounding (MIPAS) before and during the Antarctic major warming in September/October 2002, *J. Geophys. Res. Atmos.*, 109, D11307, doi:10.1029/2003JD004440, 2004.
- Hanson, D. and Mauersberger, K.: Solubility and equilibrium vapor pressures of HCl dissolved in polar stratospheric cloud materials - Ice and the trihydrate of nitric acid, *Geophys. Res. Lett.*, 15, 1507–1510, doi:10.1029/GL015i013p01507, 1988.
- Harris, N. R. P., Lehmann, R., Rex, M., and von der Gathen, P.: A closer look at Arctic ozone loss and polar stratospheric clouds, *Atmos. Chem. Phys.*, 10, 8499–8510, doi:10.5194/acp-10-8499-2010, 2010.
- Höpfner, M., Luo, B. P., Massoli, P., Cairo, F., Spang, R., Snels, M., di Donfrancesco, G., Stiller, G., von Clarmann, T., Fischer, H., and Biermann, U.: Spectroscopic evidence for NAT, STS, and ice in MIPAS infrared limb emission measurements of po-

- lar stratospheric clouds, *Atmos. Chem. Phys.*, 6, 1201–1219, doi:10.5194/acp-6-1201-2006, 2006.
- Höpfner, M., Pitts, M. C., and Poole, L. R.: Comparison between CALIPSO and MIPAS observations of polar stratospheric clouds, *J. Geophys. Res. Atmos.*, 114, D00H05, doi:10.1029/2009JD012114, 2009.
- Hurwitz, M. M., Newman, P. A., and Garfinkel, C. I.: The Arctic vortex in March 2011: a dynamical perspective, *Atmos. Chem. Phys.*, 11, 11447–11453, doi:10.5194/acp-11-11447-2011, 2011.
- Kiefer, M., Arnone, E., Dudhia, A., Carlotti, M., Castelli, E., von Clarmann, T., Dinelli, B. M., Kleinert, A., Linden, A., Milz, M., Papandrea, E., and Stiller, G.: Impact of temperature field inhomogeneities on the retrieval of atmospheric species from MIPAS IR limb emission spectra, *Atmos. Meas. Tech.*, 3, 1487–1507, doi:10.5194/amt-3-1487-2010, 2010.
- Kuttippurath, J., Godin-Beekmann, S., Lefèvre, F., and Goutail, F.: Spatial, temporal, and vertical variability of polar stratospheric ozone loss in the Arctic winters 2004/2005–2009/2010, *Atmos. Chem. Phys.*, 10, 9915–9930, doi:10.5194/acp-10-9915-2010, 2010.
- Manney, G., Santee, M. L., Rex, M., Livesey, N. J., Pitts, M. C., Veefkind, P., Nash, E. R., Wohltmann, I., Lehmann, R., Froidevaux, L., Poole, L. R., Schoeberl, M. R., Haffner, D. P., Davies, J., Dorokhov, V., Gernandt, H., Johnson, B., Kivi, R., Kyrö, E., Larsen, N., Levelt, P. F., Makshtas, A., McElroy, C. T., Nakajima, H., Parrondo, M. C., Tarasick, D. W., von der Gathen, P., Walker, K. A., and Zinoviev, N. S.: Unprecedented Arctic ozone loss in 2011, *Nature*, 478, 469–475, doi:10.1038/nature10556, 2011.
- Manney, G. L., Zurek, R. W., O'Neill, A., and Swinbank, R.: On the Motion of Air through the Stratospheric Polar Vortex, *J. Atmos. Sci.*, 51, 2973–2994, doi:10.1175/1520-0469(1994)051<2973:OTMOAT>2.0.CO;2, 1994.
- Manney, G. L., Santee, M. L., Froidevaux, L., Waters, J. W., and Zurek, R. W.: Polar vortex conditions during the 1995–96 Arctic winter: Meteorology and MLS ozone, *Geophys. Res. Lett.*, 23, 3203–3206, doi:10.1029/96GL02453, 1996.
- Manney, G. L., Santee, M. L., Froidevaux, L., Hoppel, K., Livesey, N. J., and Waters, J. W.: EOS MLS observations of ozone loss in the 2004–2005 Arctic winter, *Geophys. Res. Lett.*, 33, L04802, doi:10.1029/2005GL024494, 2006.
- Massoli, P., Maturilli, M., and Neuber, R.: Climatology of Arctic polar stratospheric clouds as measured by lidar in Ny-Ålesund, Spitsbergen (79° N, 12° E), *J. Geophys. Res. Atmos.*, 111, D09206, doi:10.1029/2005JD005840, 2006.
- Maturilli, M., Neuber, R., Massoli, P., Cairo, F., Adriani, A., Moriconi, M. L., and di Donfrancesco, G.: Differences in Arctic and Antarctic PSC occurrence as observed by lidar in Ny-Ålesund (79° N, 12° E) and McMurdo (78° S, 167° E), *Atmos. Chem. Phys.*, 5, 2081–2090, doi:10.5194/acp-5-2081-2005, 2005.
- Molina, M. J., Tso, T., Molina, L. T., and Wang, F. C.-A.: Antarctic Stratospheric Chemistry of Chlorine Nitrate, Hydrogen Chloride, and Ice: Release of Active Chlorine, *Science*, 238, 1253–1257, doi:10.1126/science.238.4831.1253, 1987.
- Newman, P. A., Gleason, J. F., McPeters, R. D., and Stolarski, R. S.: Anomalously low ozone over the Arctic, *Geophys. Res. Lett.*, 24, 2689–2692, doi:10.1029/97GL52831, 1997.
- Papandrea, E., Arnone, E., Brizzi, G., Carlotti, M., Castelli, E., Dinelli, B. M., and Ridolfi, M.: Two-dimensional tomographic retrieval of MIPAS/ENVISAT measurements of ozone and related species, *Int. J. Remote Sens.*, 31, 477–483, doi:10.1080/01431160902893501, 2010.
- Pitts, M. C., Poole, L. R., Dörnbrack, A., and Thomason, L. W.: The 2009–2010 Arctic polar stratospheric cloud season: a CALIPSO perspective, *Atmos. Chem. Phys.*, 11, 2161–2177, doi:10.5194/acp-11-2161-2011, 2011.
- Poole, L. R. and Pitts, M. C.: Polar stratospheric cloud climatology based on Stratospheric Aerosol Measurement II observations from 1978 to 1989, *J. Geophys. Res.*, 991, 13083–13090, doi:10.1029/94JD00411, 1994.
- Proffitt, M. H., Margitan, J. J., Kelly, K. K., Loewenstein, M., Podolske, J. R., and Chan, K. R.: Ozone loss in the Arctic polar vortex inferred from high-altitude aircraft measurements, *Nature*, 347, 31–36, doi:10.1038/347031a0, 1990.
- Randel, W. J. and Wu, F.: Cooling of the Arctic and Antarctic Polar Stratospheres due to Ozone Depletion, *J. Climate*, 12, 1467–1479, doi:10.1175/1520-0442(1999)012<1467:COTAAA>2.0.CO;2, 1999.
- Rex, M., Salawitch, R. J., Harris, N. R. P., von der Gathen, P., Braathen, G. O., Schulz, A., Deckelmann, H., Chipperfield, M., Sinnhuber, B.-M., Reimer, E., Alfier, R., Bevilacqua, R., Hoppel, K., Fromm, M., Lumpe, J., Küllmann, H., Kleinböhl, A., Bremer, H., von König, M., Künzi, K., Toohey, D., Vömel, H., Richard, E., Aikin, K., Jost, H., Greenblatt, J. B., Loewenstein, M., Podolske, J. R., Webster, C. R., Flesch, G. J., Scott, D. C., Herman, R. L., Elkins, J. W., Ray, E. A., Moore, F. L., Hurst, D. F., Romashkin, P., Toon, G. C., Sen, B., Margitan, J. J., Wennberg, P., Neuber, R., Allart, M., Bojkov, B. R., Claude, H., Davies, J., Davies, W., De Backer, H., Dier, H., Dorokhov, V., Fast, H., Kondo, Y., Kyrö, E., Litynska, Z., Mikkelsen, I. S., Molyneux, M. J., Moran, E., Nagai, T., Nakane, H., Parrondo, C., Ravagnani, F., Skrivankova, P., Viatte, P., and Yushkov, V.: Chemical depletion of Arctic ozone in winter 1999/2000, *J. Geophys. Res. Atmos.*, 107, 8276, doi:10.1029/2001JD000533, 2002.
- Rex, M., Salawitch, R. J., Deckelmann, H., von der Gathen, P., Harris, N. R. P., Chipperfield, M. P., Naujokat, B., Reimer, E., Allaart, M., Andersen, S. B., Bevilacqua, R., Braathen, G. O., Claude, H., Davies, J., De Backer, H., Dier, H., Dorokhov, V., Fast, H., Gerding, M., Godin-Beekmann, S., Hoppel, K., Johnson, B., Kyrö, E., Litynska, Z., Moore, D., Nakane, H., Parrondo, M. C., Risley, A. D., Skrivankova, P., Stübi, R., Viatte, P., V. Yushkov and Zerefos, C.: Arctic winter 2005: Implications for stratospheric ozone loss and climate change, *Geophys. Res. Lett.*, 33, L23808, doi:10.1029/2006GL026731, 2006.
- Santee, M. L., MacKenzie, I. A., Manney, G. L., Chipperfield, M. P., Bernath, P. F., Walker, K. A., Boone, C. D., Froidevaux, L., Livesey, N. J., and Waters, J. W.: A study of stratospheric chlorine partitioning based on new satellite measurements and modeling, *J. Geophys. Res. Atmos.*, 113, D12307, doi:10.1029/2007JD009057, 2008.
- Sinnhuber, B.-M., Stiller, G., Ruhnke, R., von Clarmann, T., Kellmann, S., and Aschmann, J.: Arctic winter 2010/2011 at the brink of an ozone hole, *Geophys. Res. Lett.*, 38, L24814, doi:10.1029/2011GL049784, 2011.
- Solomon, S.: Stratospheric ozone depletion: A review of concepts and history, *Rev. Geophys.*, 37, 275–316, doi:10.1029/1999RG900008, 1999.

- Solomon, S., Garcia, R. R., Rowland, F. S., and Wuebbles, D. J.: On the depletion of Antarctic ozone, *Nature*, 321, 755–758, doi:10.1038/321755a0, 1986.
- Spang, R. and Remedios, J. J.: Observations of a distinctive infrared spectral feature in the atmospheric spectra of polar stratospheric clouds measured by the CRISTA instrument, *Geophys. Res. Lett.*, 30, 1875, doi:10.1029/2003GL017231, 2003.
- Spang, R., Riese, M., and Offermann, D.: CRISTA-2 observations of the south polar vortex in winter 1997: A new dataset for polar process studies, *Geophys. Res. Lett.*, 28, 3159–3162, doi:10.1029/2000GL012374, 2001.
- Spang, R., Remedios, J. J., Kramer, L. J., Poole, L. R., Fromm, M. D., Müller, M., Baumgarten, G., and Konopka, P.: Polar stratospheric cloud observations by MIPAS on ENVISAT: detection method, validation and analysis of the northern hemisphere winter 2002/2003, *Atmos. Chem. Phys.*, 5, 679–692, doi:10.5194/acp-5-679-2005, 2005.
- Stein, B., Wedekind, C., Wille, H., Immler, F., Müller, M., Wöste, L., del Guasta, M., Morandi, M., Stefanutti, L., Antonelli, A., Agostini, P., Rizi, V., Readelli, G., Mitev, V., Matthey, R., Kivi, R., and Kyrö, E.: Optical classification, existence temperatures, and coexistence of different polar stratospheric cloud types, *J. Geophys. Res.*, 1042, 23983–23994, doi:10.1029/1999JD900064, 1999.
- Stiller, G. P., Mengistu Tsidu, G., von Clarmann, T., Glatthor, N., Höpfner, M., Kellmann, S., Linden, A., Ruhnke, R., Fischer, H., López-Puertas, M., Funke, B., and Gil-López, S.: An enhanced HNO₃ second maximum in the Antarctic midwinter upper stratosphere 2003, *J. Geophys. Res. Atmos.*, 110, D20303, doi:10.1029/2005JD006011, 2005.
- Tilmes, S., Müller, R., Engel, A., Rex, M., and Russell III, J. M.: Chemical ozone loss in the Arctic and Antarctic stratosphere between 1992 and 2005, *Geophys. Res. Lett.*, 33, L20812, doi:10.1029/2006GL026925, 2006.
- Tomasi, C., Petkov, B., Dinelli, B. M., Castelli, E., Arnone, E., and Papandrea, E.: Monthly mean vertical profiles of pressure, temperature and water vapour volume mixing ratio in the polar stratosphere and low mesosphere from a multi-year set of MIPAS-ENVISAT limb-scanning measurements, *J. Atmos. Sol-Terr. Phys.*, 73, 2237–2271, doi:10.1016/j.jastp.2011.06.018, 2011.
- Weisser, C., Mauersberger, K., Schreiner, J., Larsen, N., Cairo, F., Adriani, A., Ovarlez, J., and Deshler, T.: Composition analysis of liquid particles in the Arctic stratosphere under synoptic conditions, *Atmos. Chem. Phys.*, 6, 689–696, doi:10.5194/acp-6-689-2006, 2006.
- WMO: Scientific Assessment of Ozone Depletion: 2010, Global Ozone Monitoring and Research Project-Report, Project-Report 52, World Meteorological Organisation, Geneva, Switzerland, 516 pp., 2011.